Available online at www.sciencedirect.com

ScienceDirect

Procedia CIRP 108 (2022) 507–512

www.elsevier.com/locate/procedia

6th CIRP Conference on Surface Integrity

Small-scale mechanical response at intermediate/high temperature of 3D printed WC-Co

Guiomar Riu[a], Joan Josep Roa[a,*]

[a]STEROS GPA INNOVATIVE, S.L.U., C/ Maracaibo, 1, sheds 2-6, 08030 Barcelona, Spain

* Corresponding author. Tel.: +34 931 256 536; *E-mail address:* jj.roa@gpainnova.com

Abstract

The present work is focused on WC-Co dry-electropolished. A systematic nanomechanical study of a 3D printed WC-Co grade is investigated. In doing so, nanoindentation technique is implemented and the main deformation/damage mechanisms induced at the submicrometric length scale are investigated at different temperatures, from room up to 600 ºC. In general, three different approaches are followed to accomplish this research: (1) assessment of intrinsic hardness values as a function of crystallographic orientation from a room temperature up to 600 ºC and (2) the determination of effective hardness and flow stress through the Tabor's equation of the metal cobalt binder. Finally, the elastic strain to break was also determined for the main crystallographic orientations for the WC particles as a function of the temperature. The preliminary results highlight that the strength reduction with increasing temperature is attributed to metallic binder softening. On the other hand, the WC particles presents an isotropic behavior when the testing temperature is over 500 ºC because, to inside these particles, the dislocations and the stacking faults are the main deformation mechanisms induced at intermediate/high testing temperature.

Keywords: 3D printed WC-Co; DryLyte® Technology; surface integrity at high temperature

1. Introduction

Additive manufacturing (AM) technology is increasingly considered as a key manufacturing technology of tomorrow's society. AM technologies make possible the production of complex near-set shaped parts which are not feasible with conventional (subtractive) technologies. With this bottom-up approach, material is added layer by layer where necessary and it is not removed as it is with conventional top-down approaches. This technology offers many key advantages: greater design freedom compared to conventional routes, the possibility of creating close channels to optimize the cooling process under service-like working conditions, the possibility of saving on raw material consumption, production time reduction (complex parts can be produced layer by layer in just a few hours in additive machines) and no need of using customized tools. Thanks to these advantages, the use of the AM technology is being developed in many industries, like biomedical and electronics ones, as well as within scientific fields, such as mechanical devices, periodic microstructures and ceramics among others. Within the aforementioned information, the growth of activities in this field are enormous, especially with ceramic/metal printing and in particular to the WC-Co field, producing fully dense WC-Co by using the direct selective laser sintering (SLS)/selective laser melting (SLM) as reported in Refs. [1-4]. Both production techniques do not allow the normal liquid phase sintering steps, which may be associated with the very fast and local cycle of heating and subsequently solidification process. This effect may induce decarburization of WC grains, formation of carbides like W_2C and/or Co metallic binder evaporation, which affects the mechanical integrity of the 3D

10.1016/j.procir.2022.03.079

printed specimen. In order to avoid these problems, the binder jetting technology of WC-Co has been recently implemented [5,6]. It produces green parts at room temperature with no need of protective atmosphere. Afterwards, the green printed parts need further consolidation by debinding and sintering steps.

These materials under service-like working conditions can be subjected to temperatures higher than 500 ºC [7]. Due to the exceptional combination of different microstructural and mechanical properties of each constitutive phase, these materials are widely employed as cutting. At these temperatures, the mechanical properties of WC-Co drop considerably, leading to a reduction of their strength and creep resistance. This effect may be associated to microstructural (i.e., chemical composition of the metallic Co binder, mean free path, etc.), mechanical (i.e., the applied load and also the deformation rate) and thermal properties (i.e., temperature and environment) [8]. These properties produce an early deformation of the hard metal due to a softening effect of the metallic Co binder [9,10]. However, scarce information on the local mechanical properties for each constitutive phase at the micro- and submicrometric length scale is available in the literature. Within this context, the main goal behind this research is to evaluate and correlate the surface integrity in terms of mechanical properties (hardness and elastic modulus) under service-like working conditions, from room up to 600 ºC for 3D printed WC-Co specimens produced by means of the binder jetting technology and subsequently polished by using the DryLyte® Technology. Furthermore, the flow stress for the constrained Co binder will be estimated by combining the intrinsic hardness assessed for the metallic Co binder and subsequently treated by using the Tabor's equation.

Nomenclature

E_r	Reduce elastic modulus
E_{WC-Co}	Elastic modulus for the WC-Co material
E_{cBN} (T)	Elastic modulus for the cBN indenter tip as a function of the temperature
H	Hardness
H_c	Hardness for the WC-Co composite
H_f	Hardness for the metallic Co binder
H_s	Hardness for the WC particles
k	Constant related to the film thickness
SF	Stacking Fault
β	Relative indentation depth
ν_{WC-Co}	Poisson's ratio for the WC-Co material
ν_{cBN}	Poisson's ratio for the cBN indenter tip
σ_y	Flow stress
$\sigma_{y,600ºC}$	Flow stress determined at 600 ºC

2. Experimental procedure

The investigated WC-Co (12 wt. % Co) drill bit head was supplied by HILTI AG (Schaan, Liechtenstein) and processed through the additive manufacturing technologies (see Fig. 1) and in particular by using the AM route based on ink-jet printhead. More information about the 3D printing process can be found in Refs. [11-13].

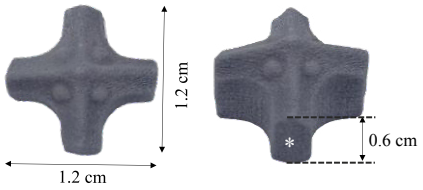

Fig. 1. 3D-printed WC-Co drill bit head.

Prior to microstructural and mechanical characterization at the submicrometric length scale, the surface of the specimen was prepared by using the dry electropolishing process, DryLyte® Technology. More information related to this polishing process is suitable in Ref. [14].

Microstructural characterization of the 3D printed specimen before being polished was performed with a confocal laser scanning microscope (CLSM, InfiniteFocusG5 plus from Bruker Alicona) and more in detail with a field emission scanning electron microscopy (FESEM, Zeiss Neon 40).

Nanoindentation tests were performed using a three-instrumented Nanotest platform (Micromaterials, Wrexham UK) equipped with a cBN Berkovich indenter (Micromaterials, Wrexham, UK) of 75 nm of the tip radius. Furthermore, along the indentation test, the cBN Berkovich indenter was carefully calibrated by indenting into a reference fused silica sample, and the obtained data were analyzed using the Oliver and Pharr method [15,16]. The indentation chamber was filled with argon gas until reaching a final O_2 level of around 1 ppm. The WC-Co composite sample was mounted on a hot stage by using Omegabond 600 (high-temperature cement) in order to carry out the experiments at room and high temperature (500 and 600 ºC). Two sets of experiments were conducted at the micro- and submicrometric length scale in the region labelled as * in Fig. 1. The overall mechanical response of the composite WC-Co grade was assessed as the average behavior of at least 20 indents per temperature conducted under loading control mode, at 25 mN of maximum applied load (with a maximum penetration depth of around 200 nm). On the other hand, the intrinsic hardness and elastic modulus as a function of the main crystallographic orientations {0001}, $\{10\bar{1}0\}$ and $\{2\bar{1}\bar{1}0\}$ as well as for the metallic Co binder. The different tests were performed at the center of each WC grain and also Co pool under load control mode at 4 mN of maximum applied load (which corresponds to a displacement into a surface of around 70 nm). In order to accurately determine the elastic properties for each constituent (WC and/or Co metallic binder) at the different investigated temperatures, it is necessary to take into account the elastic deformation of the indenter tip as a function of the tested temperature since the elastic modulus of the cBN indenter tip changes with temperature [17]. The indentation tests for both sets of experiments were conducted at a constant applied load rate of around 5 $mN \cdot s^{-1}$. The Poisson's ratio for the indenter was considered to be constant and equal to 0.12 over the

range of temperatures evaluated here (from room to 600 ºC) as reported in Ref. [18]. Finally, the corrected elastic modulus was determined by using the following expression:

$$\frac{1}{E_r} = \frac{1-v_{WC}^2}{E_{WC-Co}} + \frac{1-v_{cBN}^2}{E_{cBN(T)}} \quad (1)$$

3. Results and discussion

3.1. Microstructural characterization

The topographic view obtained through the LSCM technique for the investigated 3D printed WC-Co is shown in the upper side of Fig. 2, showing a difference in height of around 2 mm. Furthermore, the different layers deposited though the binder jetting technique are clearly evident. Doing a cross section profile of around 50 measurements (see the bottom part of Fig. 2) on the region bounded by a white dash line in the topographic LSCM image is possible to determine the layer heigh which is of around 74 µm.

Fig. 3a exhibits the FESEM micrograph of the heterogeneous WC-Co microstructure at the top surface of the 3D printed specimen, labelled as *as-received* specimen. Two different phases are evident, the ceramic (light grey), and the metallic Co binder (dark grey), being this phase the minoritarian phase of the 3D printed specimen. Prior to the mechanical characterization conducted at the submicrometric length scale, the specimen was polished using the DryLyte® Technology for 1 h and the resulting microstructure observed by FESEM (Fig. 3b), reaching a final roughness of around 9 nm. This implies a reduction of around the 33.3% the initial roughness.

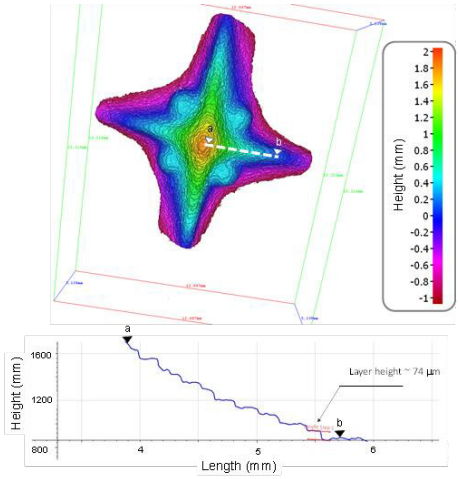

Fig. 2. Topographic LSCM image (upper) and a cross section profile (bottom).

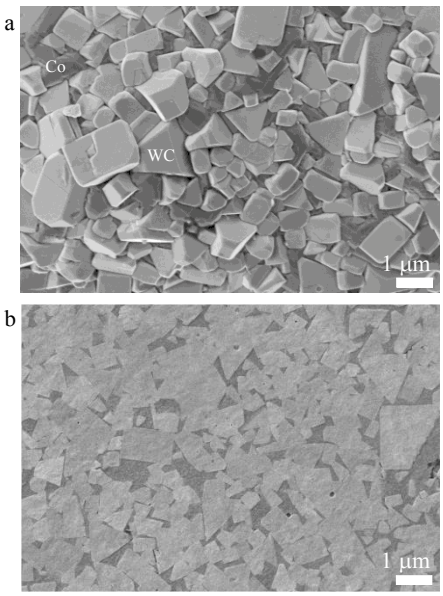

Fig. 3. FESEM micrographs of the 3D printed specimen (a) As received; and (b) after being dry-electropolished for 1 h.

3.2. Intrinsic hardness characterization for the WC particles

The evolution of the intrinsic hardness and elastic modulus as a function of the three main crystallographic orientations as a function of the testing temperature is represented in Fig 4. Ten imprints per crystallographic orientation and temperature were performed in order to get statistical signification. In this representation, it can be appreciated that both mechanical properties for the different {0001}, $\{10\bar{1}0\}$ and $\{2\bar{1}\bar{1}0\}$ orientations are temperature dependent.

The hardness for the {0001} plane measured at room temperature (see Fig. 4a) is harder than that of the other two investigated crystallographic orientations and in agreement with the data reported in the literature [19-28]. Furthermore, this representation highlights that the intrinsic hardness is a temperature dependence parameter. As it is evident, two different regions are clearly visible in the hardness vs. temperature representation, the threshold being around 500 ºC. On one hand, in region 1, the hardness for each constitutive phases presents an anisotropic behavior, being the {0001} plane harder than the other planes investigated here, $\{10\bar{1}0\}$ and $\{2\bar{1}\bar{1}0\}$. On the other hand, in region 2 (at testing temperatures higher than 500 ºC), the hardness for the three main crystallographic orientations presents an isotropic behavior with a hardness value of around 12.5 ± 0.8 GPa. The hardness behavior observed in Fig. 3a and specially in region 2 (T ≥ 500 ºC) may be related to the facility of activating the dislocation motion inside the three main WC crystallographic orientations in agreement with the data reported by Milman *et al.* [29].

Fig. 4b exhibits the elastic modulus evolution as a function of the testing temperature for the main crystallographic orientations; {0001}, $\{10\bar{1}0\}$ and $\{2\bar{1}\bar{1}0\}$. As it is shown, it linearly decreases as a function of the tested temperature. The trend obtained at room temperature is in concordance with the once obtained by using high speed massive nanoindentation

and the statistical analysis [27]. In addition, this elastic modulus reduction may be associated to heterogeneities in terms of chemical composition due to the not homogeneous distribution of W and C atoms inside the different WC particles.

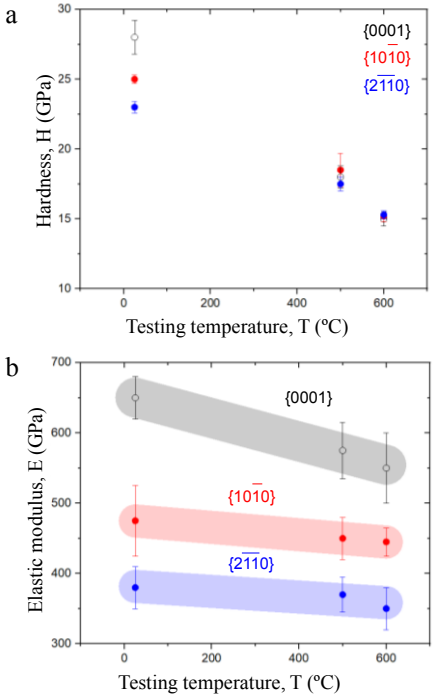

Fig. 4. Surface integrity at the submicrometric length scale for the WC particles for the three main crystallographic orientations investigated here (a) hardness; and (b) elastic modulus.

3.3. Metallic Co binder at different temperatures

The intrinsic hardness for the constrained metallic Co binder has also been investigated as a function of the tested temperatures. Table 1 summarizes the intrinsic Co hardness as a function of the temperature. As it is depicted in this table, the hardness value for the metallic Co binder is temperature dependent, leading to a reduction of this parameter as the temperature increases. This behavior may be related to two different factors: (1) a leisure of the compressive residual stresses produced due to the containment effect as the testing temperature increases and (2) the ease to activate the main plastic deformation process, being these dislocations, stacking faults (SFs) and twinning as reported in [30]. In this regard, the hardness at 600 ºC is around three times lower than that determined at room temperature. As previously reported by Roa *et al.* [25,26,28], the intrinsic hardness determined for the metallic Co binder is strongly modified by the interaction of the plastic flow induced during the indentation process with the surrounding CW. In order to deconvolute this effect and to be able to obtain a real intrinsic hardness value for the metallic Co binder, it is necessary to implement well established thin film models. In this study, the model of Korsunsky *et al.* [31] was employed by considering the WC-Co composite as the effective substrate of a metallic Co thin film as follows:

$$H_c = H_s + \frac{H_f - H_s}{1 + k\beta^2} \quad (2)$$

Values around 24% lower than those directly obtained from the indentation process on the metallic Co binder, were obtained after deconvoluting the effect of the surrounding WC particles by using the Korsunsky method as summarized in Table 1.

Table 1. Summary of the hardness as a function of the testing temperature for the metallic Co binder.

Testing temperature (ºC)	Hardness, H (*GPa*)	Hardness, H_S (*GPa*)
Room temperature	9.0 – 6.8	6.8 – 5.1
500	4.5 – 3.4	3.4 – 2.6
600	3.2 – 2.4	2.5 – 1.8

The flow stress (σ_y) for the metallic Co binder was determined from the ratio between the intrinsic hardness data after, and a constraint factor, reported to range from 3 up to 4 for WC-Co materials [32], and considering a Vickers indenter geometry. It is necessary to take into consideration that when the hardness is determined using a Berkovich tip indenter, an additional geometrical factor of 0.9 must be included in the σ_y equation as reported Casals *et al.* [33]. The σ_y evolution as a function of the temperatures investigated here (from room temperature to 600 ºC) is represented in Fig. 5. As it can be observed, σ_y and T display a clear linear relationship as represented in equation (3). As higher is the T, lower is the σ_y presented on the metallic Co binder due to a higher temperature the mobility of the main plastic deformation mechanisms is higher (i.e., mainly dislocations and SFs).

$$\sigma_y = 2.31 - 2.49 \cdot 10^{-3} \cdot T \quad (3)$$

Furthermore, the σ_y obtained at room temperature are in agreement with the data recently reported by Roa *et al.* [28,29] and Sigl and Fischmeister [34], which ranged from 1.8 to 2.4 GPa and from 2.2 to 2.6 GPa, respectively.

At the highest investigated temperature (T = 600 ºC), the σ_y obtained ranges between 0.68 up to 0.91 GPa, which is higher than the value reported for the unconstrained hard metal binder-like cobalt model alloy (0.48 GPa) [35]. On the other hand, the $\sigma_{y,600ºC}$ is in agreement with those reported in [36,37].

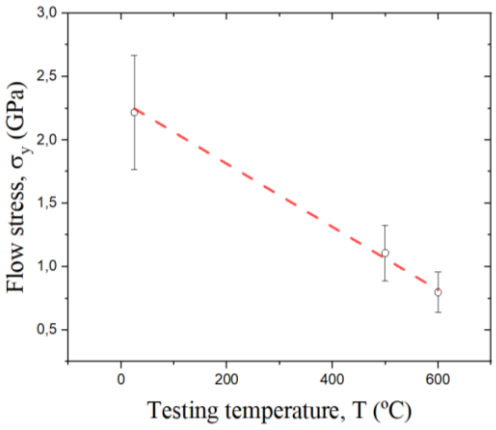

Fig. 5. Flow stress vs. indented temperature for the constrained metallic Co binder determined by using the Tabor's equation.

3.4. Plasticity parameters for the different constitutive phases

The ratio between the hardness and elastic modulus also known as a plasticity index, provides information related to the elastic strain to failure as reported in Refs. [38-41]. This parameter can be considered in indentation as an indirect measurement of toughness, especially for coated ceramic materials [44]. In this sense, the material with higher ratio can more easily relieve the strain by plastic deformation rather than brittle fracture. At the same time, this parameter can also be used as a prediction of the tribological performance of ceramic materials [45].

Table 2 summarizes the plasticity index of the main crystallographic orientations for the WC particles as a function of the tested temperature. The H/E ratio determined at room temperature ranges between $4.16 \cdot 10^{-2}$ and $6.43 \cdot 10^{-2}$ for the {0001} and $\{2\bar{1}\bar{1}0\}$, respectively. From these results it can be appreciated that the $\{2\bar{1}\bar{1}0\}$ plane should present a slightly greater wear resistance to plastic deformation than the {0001} plane. However, the difference between the main different WC planes investigated here is not high enough to be significant. As it is evident in Table 2, if the temperature increases, the elastic strain to failure reduces following the same trend for the different crystallographic planes investigated here. This phenomenon may be the result of the increase of the dislocation mobility for the different WC crystallographic phases which leads to grow the plastic deformation at the same applied stress. A similar trend was observed for a WC-Co hard metal when the testing temperature increases [46].

Table 2. Plasticity parameters for the WC particles for the main crystallographic orientation investigated.

Crystallographic orientation	Testing temperature (ºC)	$H/E \cdot 10^{-2}$
{0001}	Room temperature	4.16-4.30
	500	2.90-3.12
	600	2.58-2.84
$\{10\bar{1}0\}$	Room temperature	4.90-5.70
	500	3.85-3.86
	600	3.33-3.36
$\{2\bar{1}\bar{1}0\}$	Room temperature	5.88-6.43
	500	4.50-4.86
	600	3.89-4.47

4. Conclusions

In this work, a systematic study has been carefully implemented to dry-electropolished 3D printed WC-Co specimens with complex geometry by using the DryLyte® Technology, and subsequently evaluate the mechanical integrity for each constitutive phase (either with different nature "WC and/or Co phases" and/or crystallography "{0001}, $\{10\bar{1}0\}$ and $\{2\bar{1}\bar{1}0\}$") at different temperatures (from room temperature up to 600ºC) at the submicrometric length scale. Finally, for the constrained metallic Co binder, the flow stress has been determined by using the intrinsic hardness values and the Tabor's equation. The main conclusions extracted from this work are as follows:

(1) The mechanical properties in terms of hardness and elastic modulus determined at the submicrometric length scale are temperature dependent.
(2) The WC particles present an anisotropic behavior in terms of hardness for temperatures below 500 ºC. However, at higher temperatures the main crystallographic orientation for the WC particles presents an isotropic behavior.
(3) The elastic modulus for the different crystallographic orientations presents an anisotropic behavior being the {0001} plane the stiffest one out of all the different temperatures investigated here.
(4) The containment effect of the WC particles produces an increase of the intrinsic hardness for the metallic Co binder of around 24%.
(5) Combining the intrinsic hardness of the metallic Co binder after treating the data by using the thin film models and also the Tabor's equation allows to determine the flow stress as a function of the tested temperature.
(6) At room temperature the elastic strain to break, also known as a plasticity index, for the WC particles investigated here determined is slightly wear resistant for the $\{2\bar{1}\bar{1}0\}$ plane than for the others. Furthermore, this parameter slightly decreases when the testing temperature increases due to the required energy to activate the main plastic deformation mechanism (being these mainly the dislocations and the SFs).

Acknowledgements

Authors are grateful to HILTI AG (Schaan, Liechtenstein) to provide us the different samples investigated here. Furthermore, authors are also grateful to Zeppelin 3D metrology company (in especial to Javier Ledesma and María Gil) and the *Centro de Fabricación Avanzada Aeronáutica* (especially to Guillermo González) to conduct the 3D measurements by using the InfiniteFocusG5 plus from Bruker Alicona.

References

[1] Kumar S. Manufacturing of WC-Co moulds using SLS machine. J Mater Process Technol 2009;209:3840-48.
[2] Laoui T, Froyen L, Kruth J-P. Effect of mechanical alloying on selective laser sintering of WC-9Co powder. Powder Metall 2000;42:203-5.
[3] Domashenkov A, Borbély A, Smurov I. Structural modifications of WC/Co nanophased and conventional powders processed by selective laser melting. Mater Manuf Process. 2017;32:93-100.
[4] Uhlmann E, Bergmann A, Gridin W. Investigation on Additive Manufacturing of tunsten carbide-cobal by Selective Laser Melting, Procedia CIRP 2015;35:8-15.
[5] Enneti RK, Prough KC, Wolfe TA, Klein A, Studley N, Trasorras JL. Sintering of WC-12%Co processed by binder jet 3D printing technology. Int J Refract Met Hard Mater. 2017;71:28-35.
[6] Berger C, Abel J, Pötschke J, Moritz T. Properties of Additive Manufactured hardmetal components produced by fused filament fabrication (FFF). Proceedings of EuroPM 2018.

[7] Upadhyava GS. Cemented tunsgten carbide: production, properties and testing. New Jersey, USA: Noyes Publications. 1998.
[8] Acchar W, Gomes UU, Kaysser WA, Goring J. Strength degradation of a tunstyen carbide-cobalt composite at elevated temperatures. Mater Scharact 1999;43_27-32.
[9] Teppernegg T, Klünsner T, Kremsner C, Tritemmel C, Czettl C, Puchegger S, Marsoner S, Rippan R, Ebner R. High temperature mechanical properties of WC-Co hard metals. Int J Ref Met Hard Mat 32016;56:139-44.
[10] Emani SV, Ramos dos Santos AFC, Shar LL, Chen Z. Investigation of microstructure and mechanical properties at low and high temperatures of WC-6wt.% Co, Int J Refract Met Hard Mater 2016;58:172-81.
[11] Carreño-Moreli E, Alveen P, Moseley S, Rodriguez-Arbaizar M, Cardoso K. A comparative study of cemented carbide parts produced by solvent on granules 3D-printing (SG-3DP) versus press and sinter. Int J Refract Met Hard Mater 2021;97:105515/1-6.
[12] Carreño-Moreli E, Martineri S, Bidaux JE. Granules for three dimensional printing. 2005. European patent application EP05109045.4.
[13] Carreño-Moreli E, Alveen P, Moseley S, Rodriguez-Arbaizar M, Cardoso K. Three-dimensional printing of hard materials. Int J Refract Met Hard Mater 2020;87:105510/1-6.
[14] P202130985. Sarsanedas M., Riu G, Roa JJ. Medio electrolítico para electopulido y método de electropulido con dicho medio 2021.
[15] Oliver WC, Pharr GM. Improved technique for determining hardness and elastic modulus using load and displacement sensing indentation experiments. J Mater Res 1992;7:1564-80.
[16] Oliver WC, Pharr GM. Measurement of hardness and elastic modulus by instrumented indentation: advances in understanding and refinements to methodology. J Mater Res 2004;19:3-20.
[17] Ctvrtlik R, Al-Haik MS, Kulikovsky V. Mechanical properties of amorphous silicon carbonitride thin films at elevated temperatures. J Mater Sci 2015;50:1553-64.
[18] D'Evelyn MP, Taniguchi T. Elastic properties of translucent polycrystalline cubic boron nitride as characterized by the dynamic resonance method. Diam Relat Mater 1999;8:1522-6.
[19] Acchar W, Gomes UU, Kaysser WA, Goring J. Strength degradation of a tungsten carbide-cobalt composite at elevated temperatures. Mater Charact 1999;43:27-32.
[20] French DN, Thomas D, Hardness anisotropy and slip in WC crystals. Trans AIME 1965;14A:1625-29.
[21] Cuadrado N, Casellas D, Llanes L, González I, Caro J. Effect of crystal anisotropy on the mechanical properties of WC embedded in WC-Co cemented carbides, in: Proceedings of the Euro PM2011-Hard Materials, Barcelona 2011;2:215-20.
[22] Roebuck B, Klose P, Mingard KP. Hardness of hexagonal tungsten carbide crystals as a function of orientation. Acta Mater 2012;60:6131-43.
[23] Duszová A, Halgas R, Bl'anda M, Hvizdos P, Lofaj F, Dusza J, Morgiel J. Nanoindentation of WC-Co hardmetals. J Eur Ceram Soc 2013;33:2227-32.
[24] Csanádi T, Blánda M, Chinj NQ, Hviszdos P, Dusza J. Orientation-dependent hardness and nanoindentation-induced deformation mechanisms of WC crystals. Acta Mater 2015;83:397-407.
[25] Roa JJ, Jiménez-Piqué E, Tarragó JM, Sandoval DA, Mateo A, Fair J, Llanes L. Hall-Petch strengthening of the constrained metallic binder in WC-Co cemented carbides: Experimental assessment by means of massive nanoindentation and statistical analysis. Mat Sci Eng A 2016;676:487-91.
[26] Roa JJ, Jiménez-Piqué E, Verge C, Tarragó JM, Mateo A, Fair J, Llanes L. Intrinsic hardness of constitutive phases in WC-Co composites: Nanoindentation testing, statistical analysis, WC crystal orientation effects and flow stress for the constrained metallic binder. J Eur Ceram Soc 2015;35:3419-25.
[27] Roa JJ, Sudharshan Phani P, Oliver WC, Llanes L. Mapping of mechanical properties at microstructural length scale in WC-Co cemented carbides: Assessment of hardness and elastic modulus by means of high speed massive nanoindentation and statistical analysis. Int J Refrac Met Hard Mater 2018;75:211-7.
[28] Roa JJ, Mateo AM, Llanes L. Implementation of massive nanoindentation coupled with statistical analysis to evaluate complex heterogeneous microstructures in materials manufactured following powder metallurgy processing routes. Encyclopedia of Materials: Metals and Alloys 2021; pp. 465-70.
[29] Milman YV, Lyckx S, Goncharuck VA, Northrop JT. Results from bengins tests on submicron and micron WC-Co grades at elevated temperatures. Int J Refract Met Hard Mater 2002;20:71-9.
[30] Roa JJ, Jiménez-Piqué E, Tarragó JM, Zivcec M, Broeckmann C, Llanes L. Berkovich nanoindentation and deformation mechanisms in a hardmetal binder-like cobalt alloy. Mater Sci Eng A 2015;621:128-32.
[31] Korsunsky AM, McGurk MR, Bull SJ, Page TF. On the hardness of coated systems. Surf Coat Technol 1998;99:171-83.
[32] Doi H, Fujiwara Y, Miyake K. Mechanism of plastic deformation and dislocation damping of cemented carbides. Trans Metall Soc AIME 1969;245:1457-70.
[33] Casals O, Alcalá J. The duality in mechanical property extractions from Vickers and Berkovich instrumented indentation experiments. Acta Mater 2005;53:3545-61.
[34] Sigl LS, Fischmeister HF. On the fracture toughness of cemented carbides. Acta Metall 1988;36:887-97.
[35] Roebuck B, Almond EA, Cottenden AM. The influence of composition, phase transformation and varying the relative F.C.C. and H.C.P. phase contents on the properties of dilute CoWC alloys. Mater Sci Eng 1984;66:179-94.
[36] Schmid HG, Mari D, Benoit W. The mechanical behaviour of cemented carbides at high temperature. Mater Sci Eng A. 1988;105/106:343-51.
[37] Novikov NV, Bondarenko VP, Golovchan VT. High-temperature mechanical properties of WC-Co Hard Metals (Review). J Superhard Mater 2007;29:261-80.
[38] Leyland A, Matthews A. Design criteria for wear-resistant nanostructured and glassy-metal coatings. Surf Coat Technol 2004;177-178:317-24.
[39] Leyland A, Matthews A. On the significance of the H/E ratio in wear controls: a nanocomposite coating approach to optimized tribological behavior. Wear 2000;46:1-11.
[40] Strauss HW, Chromik RR, Hassani S, Klemberg-Sapieha JE. In situ tribology of nanocomposite Ti-Si-C-H coatings prepared by PE-CVD. Wear 2011;272:133-48.
[41] Frutos E, Cuevas A, González-Carrasco JL, Martín F. Characterization of the elastic-plastic behavior of intermetallic coatings growth on medical stainless steel by instrumented ultramicroindentation. J Mech Beh Biomed Mater 2012;16:1-8.
[42] Bousser E, Benkahoul M, Martinu L. Effect of microstructure on the erosion resistance of Cr-Si-N coatings. Surf Coat Technol 2008;203:776-80.
[43] Gee MG, Grant A, Roebuck B. Wear mechanisms in abrasion and erosion of WC/Co and related hardmetals. Wear 2007;263:137-48.
[44] Wood BJK. Multifunctional materials for tribological applications. 1st ed., 2015. ISBN: 9780429068492.
[45] Sarkar AD. Wear of metals. 1976. ISBN: 978-0-08-019737-1.
[46] Vornberger A, Pötschke J, Gestricj T, Hermann M, Michaelis A. Influence of microstructure on hardness and thermal conductivity of hardmetals. Int J Refract Metals Hard Mater 2020;80:105170/1-105170/8.